Fragment recoil anisotropies in the photoinitiated decomposition of HNCO

M. Zyrianov, Th. Droz-Georget, and H. Reisler
Department of Chemistry, University of Southern California, Los Angeles, California 90089-0482

(Received 20 July 1998; accepted 21 October 1998)

The photofragment ion imaging technique is used to determine product recoil anisotropy parameters, β, and correlated state distributions in the $S_1(^1A'')\leftarrow S_0(^1A')$ photoinitiated decomposition of HNCO into three competing channels: (1) ^{3}NH+CO, (2) H+NCO, and (3) ^{1}NH+CO [where ^{3}NH and ^{1}NH denote NH($X\,^3\Sigma^-$) and NH($a\,^1\Delta$), respectively]. In particular, the region in the vicinity of the ^{1}NH+CO threshold is investigated. The measured recoil anisotropies fall into two distinct groups corresponding to time scales of <1 ps ($\beta<-0.6$), and $>5-10$ ps ($\beta\cong 0.0$). With 230.1 nm photolysis, CO($J=0-14$) originating in channel (3) is produced with $\beta=-0.8\pm0.05$ via direct dissociation on S_1 above a barrier of 470 ± 60 cm^{-1}. CO at low J-states appears with most of the available energy in the translational degree of freedom and is correlated with ^{1}NH in its lowest rotational states. A small contribution to channel (3) from S_0 dissociation (observed mainly for $J=14,15$) gives rise to an isotropic recoil distribution, and a hotter correlated ^{1}NH rotational distribution. At the same wavelength, CO correlated with ^{3}NH is identified by its high translational energy and exhibits an isotropic angular distribution. We propose that the pathway leading to its formation is $S_1\rightarrow S_0\rightarrow T_1$. H-atom signals from channel (2) have isotropic angular distributions at photolysis wavelengths $243-215$ nm; this places a lower limit of 8140 cm^{-1} on the barrier to direct dissociation on S_1 to channel (2). The >5 ps time scale for the appearance of channel (2) implies dissociation on S_0 following internal conversion. The mechanism described here for the one-photon decomposition of HNCO in the wavelength region 260-230 nm is in accord with other available experimental and theoretical findings. © *1999 American Institute of Physics.*
[S0021-9606(99)01704-3]

I. INTRODUCTION

Open shell molecular species such as free radicals or electronically excited molecules often exhibit multiple decay pathways. These can include chemically distinct decomposition channels, and/or radiationless decay pathways involving the breakdown of the Born Oppenheimer approximation, e.g., internal conversion (IC) and intersystem crossing (ISC).[1,2] In other words, the zero-order discrete state describing the electronically excited state couples simultaneously to several continua or quasicontinua. In principle, these processes should be described quantum mechanically in terms of resonance scattering, coupling matrix elements to the various continua, interference among competing pathways, etc. Indeed, for few molecules with modest density of states, ρ, it has been possible to observe and treat theoretically such phenomena.[1,3–9] On the other hand, when ρ is large, excitation of a single state is unlikely, and many of the quantum mechanical and state-specific effects average out, giving rise to a smooth behavior resulting from the coherent and incoherent superposition of many resonances. In such cases, the time evolution of the system can be described in terms of average rates. Regardless whether a rate picture or a description based on coupling matrix elements is invoked, decay processes are associated with characteristic time scales, and their identification is important in sorting among competing pathways. When combined with product state distributions and branching ratios, they can lead to a better understanding of the decomposition mechanisms of complex systems.

The photofragment imaging technique is particularly useful in this regard. Since the products are detected state-selectivety (e.g., by resonant laser ionization), the images afford simultaneous resolution in the frequency, velocity, and angular domains. The angular distributions are usually fit with an effective recoil anisotropy parameter, β, which characterizes the angular distribution in terms of the angle between the direction of the light polarization vector and the direction of fragment recoil.[10] The β parameter, in turn, is associated with a characteristic time scale determined relative to the average rotational period of the molecule. Although, as discussed in Sec. IV, the quantitative extraction of lifetimes from angular distributions is difficult, in favorable cases the existence of distinct time scales for different product channels can be clearly demonstrated.

In the present work, the ion imaging technique is used to characterize the time scales and mechanisms involved in the decomposition of expansion-cooled isocyanic acid (HNCO) following $S_1(^1A'')\leftarrow S_0(^1A')$ excitation. HNCO is implicated in the removal of NO_X products in a process known in combustion as REPRENO$_X$ (RAPid Reduction of NO$_X$), in energetic materials combustion and in interstellar space. Although it has only four atoms, it can serve as a benchmark for more complex systems, since at least three potential energy surfaces (S_0, T_1 and S_1) participate in its dissociation at <231 nm into three competing channels:[11–29]

$$\rightarrow \quad NH(X\,^3\Sigma^-) + CO(X\,^1\Sigma^+) \qquad D_0(^3NH+CO) = 30\,060 \pm 25 \ \text{cm}^{-1}, \tag{1}$$

$$HNCO \quad \rightarrow \quad H(^2S) + NCO(X\,^2\Pi) \qquad D_0(H+NCO) = 38\,370 \pm 30 \ \text{cm}^{-1}, \tag{2}$$

$$\rightarrow \quad NH(a\,^1\Delta) + CO(X\,^1\Sigma^+) \qquad D_0(^1NH+CO) = 42\,750 \pm 25 \ \text{cm}^{-1}. \tag{3}$$

In what follows $NH(X\,^3\Sigma^-)$ and $NH(a\,^1\Delta)$ are denoted by ^3NH and ^1NH, respectively. Threshold values are taken from Ref. 17 for channel (2) and from this work for channels (1) and (3). All channels remain open up to at least 46 000 cm^{-1} (217 nm) photolysis energy.[20] A schematic energy diagram is provided in Fig. 1.

The role of the spin-forbidden channel (1) following optical excitation has only recently been revealed,[22] although it has been previously observed in HNCO pyrolysis.[25] This channel is observed from well below the channel (2) threshold (e.g., at ~280 nm) to at least up to 46 000 cm^{-1} (217 nm). Although its exact quantum yield is unknown, it is still the major channel in the region just above the opening of channel (2).[29] The pathway responsible for its formation has not been determined.

Channel (2) dissociation up to the channel (3) threshold is thought to occur via IC to S_0.[17–20] However, the height of the barrier to direct decomposition on S_1 has not been determined experimentally, although an upper limit of ~13 000 cm^{-1} above the channel (2) barrier is suggested by studies at 193 nm.[15] Channel (3) dissociation is thought to evolve initially on S_0, but after exceeding a small barrier on S_1, estimated at 400–600 cm^{-1}, direct dissociation on this surface quickly dominates.[20,24] The quantum yield of the H+NCO channel correspondingly diminishes, and channel (3) becomes the major channel.[18,19] To establish the mechanism for its formation, especially near the threshold, it is important to minimize the overlap with the CO signal produced via channel (1). Recently, this has been achieved by exploiting the velocity discrimination afforded by the photofragment ion imaging technique.[24] We found that the CO rotational distribution is cold, having a maximum at $J_{CO}=0-2$ and decreasing rapidly at higher J's. Here we explore in greater detail the pathways responsible for channel (3). Vibrationally mediated photodissociation (VMP) experiments demonstrated that it is possible to change the branching ratios into the various channels by implanting several quanta of ν_1 vibrational excitation in the ground state prior to the electronic excitation.[23]

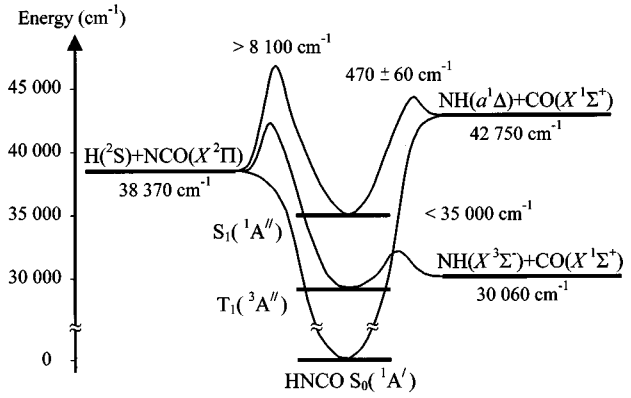

FIG. 1. Schematic energy level diagram of the three lowest energy dissociation channels of HNCO.

Theoretical calculations, mainly on the S_1 potential energy surface (PES) topology,[26–28] are in agreement with the experimental findings. However, the complexity of the photodissociation of HNCO gives rise to several possible mechanistic interpretations, and the subtle interplay among different intramolecular interactions and couplings to the dissociative continua has to be sorted out before reaching definitive conclusions. Understanding the relative strengths of these interactions is key, since they determine the time scales for intramolecular radiationless decay processes and dissociation.

In this paper we report a photofragment ion imaging study of the photodissociation of HNCO to all three channels. Near-threshold regions are especially informative regarding mechanisms, and here we concentrate on photolysis energies around 230 nm, slightly above the opening of channel (3). At this wavelength, we find markedly different CO product recoil anisotropies for dissociation via channels (1) and (3), and we argue that the mechanism for channel (1) formation is $S_1 \rightarrow S_0 \rightarrow T_1$, rather than direct $S_1 \rightarrow T_1$ coupling. Our data also reveal the competition between dissociation on S_0 and S_1 to channel (3), and provide a low limit for the barrier height to channel (2) on S_1, as well as a more accurate value for the S_1 barrier to channel (3).

In a separate study, we have found that near the channel (2) threshold, decomposition to channel (2) evolves on S_0 without a barrier, and that the rate of channel (2) formation in this energy region is much slower than the competing $S_0 \rightarrow T_1$ ISC rate.[29] In Sec. V, we summarize the results regarding the one-photon decomposition of HNCO, and provide a mechanistic interpretation that reconciles all the experimental observations at photolysis energies from below the channel (2) threshold to above the opening of direct S_1 dissociation to channel (3), and is also in accord with recent theoretical results.

II. EXPERIMENTAL DETAILS

The photofragment ion imaging arrangement has been described previously.[21,24] In brief, it consists of an ion-acceleration stage, a 60 cm long drift-tube, a position-sensitive detector and a CCD camera that monitors a phosphor screen coupled to a MCP detector. The ion-acceleration stage is used in the velocity map imaging configuration pro-

posed by Parker *et al.*[30] A repeller, an open extractor electrode, and an open ground electrode with 1.0 in. holes are used. Both the repeller and the extractor electrodes are 0.2 mm thick. At an optimal voltage ratio for the repeller and extractor plates, all ions with the same initial velocity are focused to the same spot on the MCP detector (velocity map imaging). This setup avoids image blurring due to the finite size of the laser/molecular beam interaction volume. Although in near-threshold imaging the resolution is limited by the molecular beam velocity spread, residual space charge effects, and the mechanical precision of the lens assembly, the new ion lens arrangement provides a factor of 3–5 improvement in resolution in comparison with the conventional setup.[30]

A doubly-skimmed pulsed molecular beam containing 2% HNCO seeded in 1.0 atm He enters the acceleration region through a 1.0 mm hole in the repeller plate. HNCO ($T_{\rm rot}=5$ K) is photolyzed with pulsed, linearly polarized, and focused laser radiation from an excimer laser pumped dye laser (Lambda Physik, EMG 201 or Compex 102 excimer and FL 3002 dye laser) intersecting the molecular beam at right angle. Atomic hydrogen and CO photofragments are probed either by the same laser in one-color experiments or using the counterpropagating, focused radiation of a separate probe laser (Continuum ND6000 pumped by NY81C-10 Nd:YAG laser).

The collected images represent 2D projections of the 3D spatial recoil distributions of the photofragments. All the images presented in this paper are symmetrized. The 3D distributions are then reconstructed by means of the inverse Abel transformation, and 2D cuts including the axis of symmetry are presented.[31] The velocity distributions are obtained from the 3D recoil distributions by integrating the signal for each radial distance r from the center, as described before.[21,24] In order to obtain the angular distributions, $P(\theta)$, the reconstructed 3D distributions (in polar coordinates) are integrated along ϕ and r, with θ being the angle between the recoil velocity vector and the laser polarization vector. The angular distributions are fitted to the standard recoil anisotropy function,[10]

$$P(\theta)=(2-\beta)+3\beta\cos^2\theta. \tag{4}$$

A. CO detection

CO products are interrogated by $2+1$ resonance-enhanced multiphoton ionization (REMPI) via the Q-branch of the $B\,^1\Sigma^+\leftarrow\leftarrow X\,^1\Sigma^+$ transition at 230.1 nm ($\leftarrow\leftarrow$denotes two-photon absorption).[24] This transition is free from alignment effects,[32] which simplifies the interpretation of the derived recoil anisotropy parameters. Laser radiation of 0.5–1.0 mJ focused by a 24 cm focal length (f) lens was used in the one-color experiments. For two-color experiments, the pump radiation frequency was tuned away from the CO absorption lines, and its power and focusing conditions were kept the same, while energies <100 μJ ($f=19$ cm) were used for the probe laser output. Note that owing to the velocity discrimination in the imaging experiments, the CO signals from the 1- and 2-color processes do not overlap in space (see Sec. III).

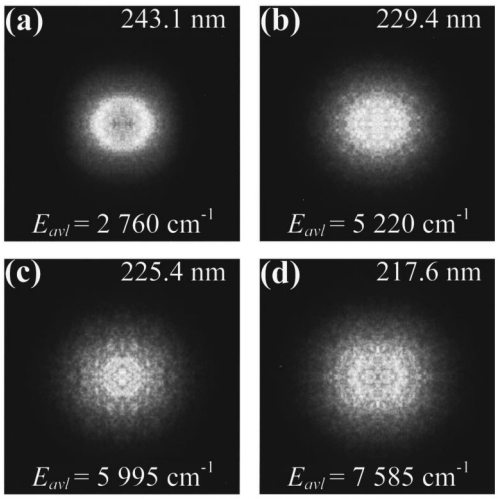

FIG. 2. Images of hydrogen atom produced in HNCO photolysis at available energies above the channel (2) threshold of (a) 2760 cm^{-1}, (b) 5220 cm^{-1}, (c) 5995 cm^{-1}, and (d) 7585 cm^{-1}. The H-atoms are monitored by $2+1$ REMPI at 243.1 nm.

B. Hydrogen detection

Hydrogen atoms are detected by $2+1$ REMPI via the $2\,^2S\leftarrow\leftarrow 1\,^2S$ transition at 243.1 nm. In the one-color experiments the $\sim$0.4 mJ laser output was focused by $f=19$ cm lens. In the two-color experiments $\sim$1.0–1.5 mJ radiation focused by $f=24$ cm lens was used to dissociate the HNCO, while $<$0.2 mJ ($f=19$ cm) was used to probe the hydrogen atoms. Since the absorption cross section of HNCO is much smaller at 243.1 nm than at 230-215 nm,[11] the background signal from the probe laser alone was insignificant compared to the combined pump and probe signal. The probe laser wavelength was scanned during the acquisition of an image over the full Doppler profile of the recoiling hydrogen. Special care was taken to ensure proper time overlap of the pump and probe laser pulses. Due to the fast recoil of the light hydrogen atoms out of the detection region, even a slight delay of the probe pulse leads to preferential detection of hydrogen atoms moving parallel to the laser beam and results in artificially elongated images. This was not observed in our experiments. The jitter in these experiments (carried out using the Compex excimer laser system) was always less than 5 ns.

III. RESULTS

A. Hydrogen fragment ion images

Figure 2 presents four images of hydrogen photofragments taken at different photolysis energies in the range 243-215 nm. Image (a) is obtained in a one-color experiment at 243.1 nm (2760 cm^{-1} above the threshold to H+NCO). Image (b) is taken near 230 nm, where substantial recoil anisotropy in the CO product originating from the ^{1}NH+CO channel has been observed previously.[21] This excitation (229.4 nm; $E_{\rm avl}=5220$ cm^{-1}) coincides with a prominent feature in the yield spectrum of the H+NCO channel.[17] Image (c) is recorded at 225.4 nm ($E_{\rm avl}=5995$ cm^{-1}), in the region where Crim and co-workers observed an enhancement of the

NCO/^{1}NH yield in VMP experiments.[23] Finally, image (d) is obtained at 217.6 nm ($E_{avl}=7585\,cm^{-1}$), near a wavelength where CO recoil distributions were reported.[16] An additional image, not shown, is taken at 215 nm ($E_{avl}=8140\,cm^{-1}$). None of the hydrogen images recorded in this study show significant angular anisotropy, with the β parameters ranging from -0.02 to -0.15. In general, such small values of β are very sensitive to the signal to noise ratio, and the variations among the derived values are insignificant. Additionally, a semiclassical model that takes into account rotation of the parent molecule shows that the limiting value of β for infinitely slow dissociation is -0.23 (rather than zero) for the perpendicular $S_1\leftarrow S_0$ transition in HNCO (*vide infra*).[33]

B. CO($X\,^1\Sigma^+$) product ion images

In a preliminary publication we obtained the rotational distribution of the CO fragment at 230 nm, and discussed the images obtained for CO($J=0-2$).[24] In this work we extend the measurements to high J_{CO} states and measure the anisotropy as a function of CO velocity. Shown in Figs. 3(a) and 3(b) are two images obtained in a one-color experiment at 230.1 nm for selected rotational levels of the CO product. The *Q*-branch of the $B\,^1\Sigma^+\leftarrow\leftarrow X\,^1\Sigma^+$ transition used for CO detection is severely collapsed for low *J*'s. Although for $J_{CO}>10$ the congestion diminishes, it is not possible to excite a single *J* level without residual contributions from neighboring states. Consequently, $J_{CO}=14,15$ and $J_{CO}=12,13$ are monitored for the images shown in Figs. 3(a) and 3(b), respectively. Panels (c) and (d) represent 2D cuts in their respective inverse Abel transforms, and the corresponding velocity distributions are shown on panels (e) and (d).

With 230.1 nm photolysis, the CO product can originate from both the spin-allowed [channel (3)] and spin-forbidden [channel (1)] pathways. The velocity distributions were modeled as described before,[20,24] taking into account only the spin-allowed channel. This is shown in thin solid lines in panels (e) and (f). $J_{CO}=14$ and 15 are found to contribute in the ratio of 5:1 to the distribution on panel (e). The rotational levels of the correlated ^{1}NH cofragment are well resolved, and all the energetically allowed levels are significantly populated. The distribution in panel (f) is best modeled with a 2:1 ratio of $J_{CO}=12$ and 13. The resolution of the ^{1}NH cofragment rotational levels is poorer, partly due to the comparable admixture of the two rotational levels of CO. Note that there is clear propensity to populate low *J* states of ^{1}NH in this distribution; e.g., $J_{NH}=5$, which is energetically allowed for $J_{CO}=12$, does not appear in the distribution. The feature visible at around 0.5 mm/μs in both velocity distributions is not compatible in terms of energy conservation with the formation of channel (3) following electronic excitation from the ground vibrational state of HNCO(S_0). On the other hand, this feature can be fit well by assuming excitation of HNCO(S_0) out of the $v_5=1$ vibrational state which lies at 577 cm^{-1}. The intensity between the peaks derives from CO produced via channel (1) (not included in the modeling), whose translational energy extends to the limit allowed by the available energy (see below).

The recoil anisotropy parameters derived from the transforms (c) and (d) differ significantly. In the former, the rings correlated with $J_{NH}=3$ and 4 are nearly isotropic, the ring correlated with $J_{NH}=2$ shows slight anisotropy, whereas the outermost ring correlated with $v_5=1$ excitation is clearly anisotropic. In contrast, the β parameters extracted for the different rings present in image (d) are all more negative than -0.6.

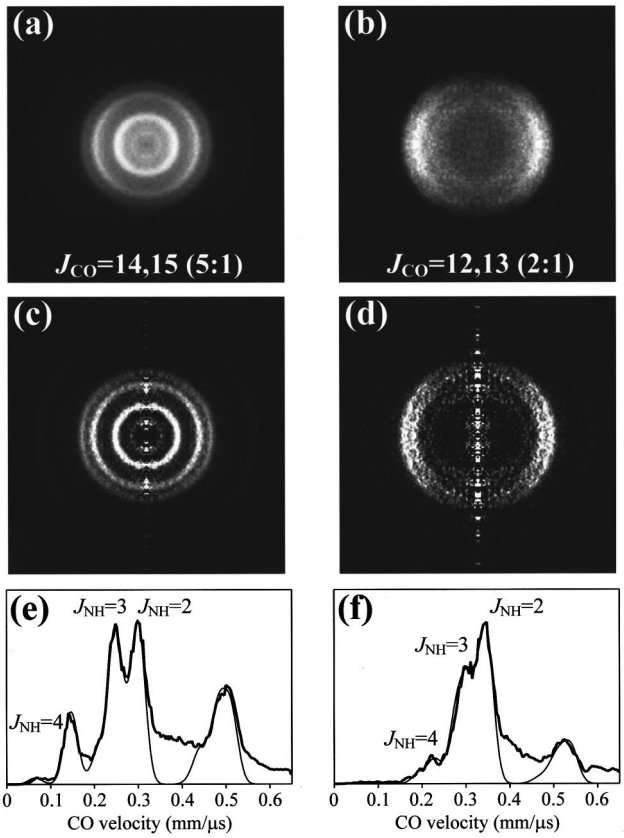

FIG. 3. CO images obtained via 2+1 REMPI at ~230.1 nm in a one-color experiment monitoring (a) $J_{CO}=14,15$ and (b) $J_{CO}=12,13$. Panels (c) and (d) represent 2D cuts (including the axis of cylindrical symmetry) through the 3D velocity distributions, obtained using the inverse Abel transform of images (a) and (b), respectively. In panels (e) and (f) the corresponding velocity distributions derived from the reconstructed 3D images are shown in thick lines. The thin solid lines show fits to the velocity distributions, assuming that the CO signals derive solely from dissociation to channel (3) (see the text). The observed residual intensity between the peaks at the high velocity end originates in faster CO correlated with channel (1). Note that the rings corresponding to the features at ~0.5 mm/μs in panels (e) and (f) are not visible in the images and Abel transforms due to insufficient dynamic range of image reproduction.

We should note that the best fits to the velocity distributions in Figs. 3(e) and 3(f) are obtained by using $D_0(^1\text{NH}+\text{CO})=42\,750\,cm^{-1}$. This value is 15 cm^{-1} lower than the value derived previously from lower resolution imaging data.[21] Considering the much higher resolution of the velocity map imaging employed here, the new value, $D_0(^1\text{NH}+\text{CO})=42\,750\pm25\,cm^{-1}$, is preferred. The channel (1) threshold should be corrected accordingly to $D_0(^3\text{NH}+\text{CO})=30\,060\,cm^{-1}$, as it is obtained by the subtraction of the NH($X\,^3\Sigma^-$) and NH($a\,^1\Delta$) electronic levels separation from the channel (3) threshold.[17]

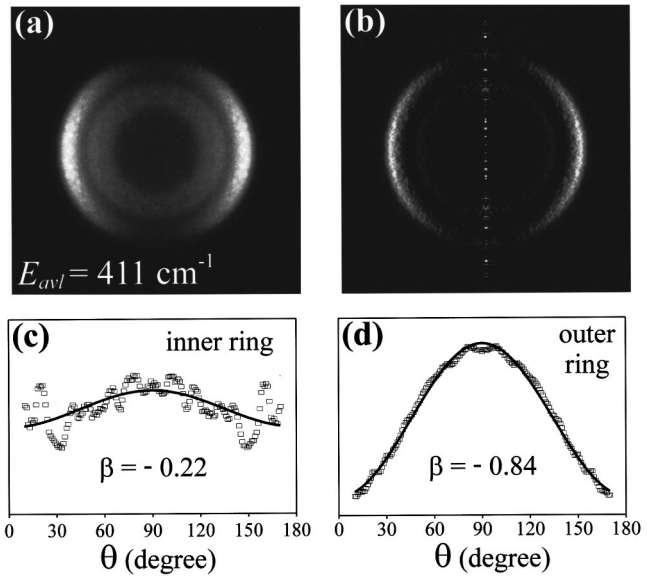

FIG. 4. (a) CO image and (b) 2D cut of its Abel-transform obtained in a two-color experiment at photolysis energy 411 cm^{-1} above the channel (3) threshold (231.7 nm). Angular distributions (open squares) and their fits (solid lines) are shown in (c) and (d) for the inner and outer rings, respectively.

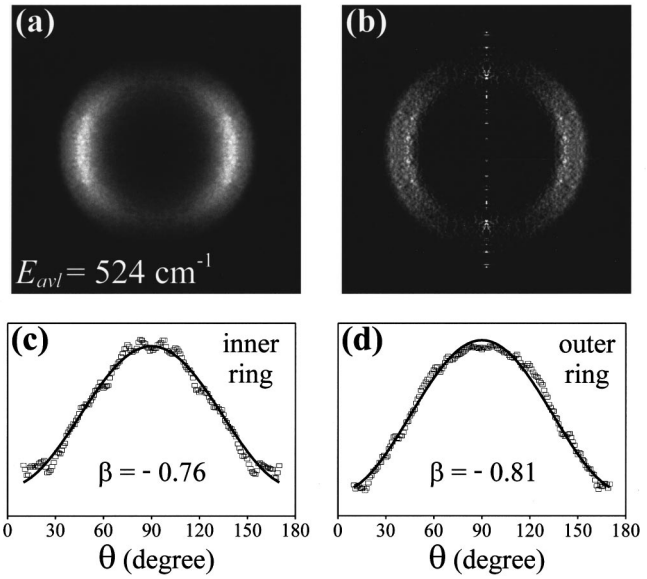

FIG. 5. (a) CO image and (b) 2D cut of its Abel-transform obtained in a two-color experiment at photolysis energy 524 cm^{-1} above the channel (3) threshold (231.1 nm). Angular distributions (open squares) and their fits (solid lines) are shown in (c) and (d) for the inner and outer rings, respectively.

Figure 4(a) presents an image of the CO fragment obtained in a two-color experiment with the photolysis energy 411 cm^{-1} above the ^{1}NH+CO threshold. The CO *Q*-branch bandhead consisting of low J_{CO} was monitored in this experiment. Of the two rings visible in the image, the outer one is associated with the probe laser only (and is similar to the one-color experiment at 230.1 nm reported earlier),[24] and the inner ring is the two-color signal of interest. Panel (b) presents a 2D cut of the inverse Abel transform of image (a), in which the separation of the two rings is clearly visible. The angular distributions are shown as open squares on panels (c) and (d), respectively. The recoil anisotropies for the inner and outer rings are markedly different. The anisotropy parameter fit corresponds to $\beta=-0.84$ for the one-color signal and $\beta=-0.22$ for the two-color signal. Taking into account the signal to noise ratio of the two-color experiment and the arguments made earlier for close-to-zero values of β, the latter value corresponds to no anisotropy.

Figure 5 presents results similar to those of Fig. 4, but with the photolysis energy set to 524 cm^{-1} above the ^{1}NH+CO threshold. The particular choice of the excitation energies coincides with the location of two adjacent peaks in the ^{1}NH yield spectrum.[17] Although the separation of the inner and the outer rings is not as complete as in the previous case, it is still sufficient for separate determinations of the corresponding anisotropy parameters. The fits correspond to $\beta=-0.81$ and -0.76 for the one- and two-color signals, respectively.

Shown in Fig. 6 are two views of the image obtained in a one-color experiment at 230.1 nm, in which the CO *Q*-branch bandhead consisting of low J_{CO} was monitored, and the ion-optics acceleration voltage was set such that all CO fragments originating from both channels (1) and (3) were imaged on the detector simultaneously. The central part of image (a) displays CO products correlated with ^{1}NH, as observed in a previous velocity-map imaging one-color experiment.[24] Panel (b) presents another view of the same image, obtained with an intensity scaling that highlights the outer ring, which arises from the CO generated via channel (1). Panels (c) and (d) show the angular distributions associated with the central and the outer parts of the image, respectively. While CO originating from the spin-allowed channel yields $\beta=-0.78$, the recoil of CO originating from the spin-

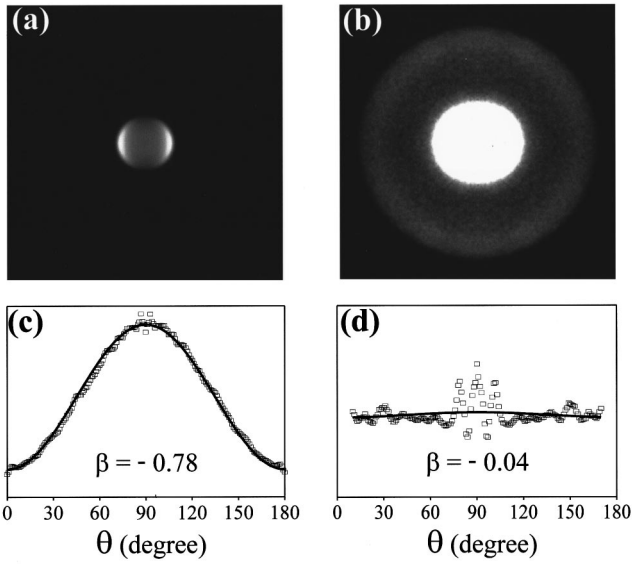

FIG. 6. Panels (a) and (b) display two views of the CO image obtained in a one-color experiment at 230.1 nm by monitoring low J_{CO}. The image is shown on different scales to highlight the central [channel (3)] and outer [channel (1)] parts (see the text). Angular distributions (open squares) and fits (solid lines) are shown in (c) and (d) for the central and outer parts, respectively.

forbidden channel (1) is essentially isotropic. The outer rings of the images taken for $J_{CO}=15$ and 30 (not shown) are also isotropic.

IV. DISCUSSION

A. Photofragment recoil anisotropy and dissociation time scales

Photofragment angular distribution measurements can provide estimates of dissociation lifetimes with respect to the rotational period of the parent molecule.[10] However, the conversion of the β parameters that best fit the data to fragment appearance times is not straightforward. Several authors discussed how finite dissociation lifetimes, nonaxial recoil and out-of-plane vibrations affect β in a rotating and dissociating molecule.[33–40] The results of these studies, in which both classical and quantum models are considered, are summarized in a recent review by Gordon and Hall.[33]

In the classical treatments, the dissociating molecule is treated as a rigid rotating pseudodiatomic decaying with a characteristic lifetime.[35–37] While the limiting values of β in fast dissociation (assuming axial recoil) are $+2$ and -1 for parallel and perpendicular transitions, respectively,[10] these values are reduced fourfold in the slow dissociation limit.[35,36] This gives $\beta=0.5$ and -0.25 for parallel and perpendicular transitions, respectively. Yang and Bersohn, who extended the classical treatment to spherical and symmetric top molecules, found that in the slow dissociation limit β was reduced by a factor of 4–5.9, depending on the ratio of the moments of inertia of the top.[37] For HNCO, this factor is 4.35, corresponding to $\beta=-0.23$ in the slow dissociation limit for the perpendicular $S_1(^1A'')\leftarrow S_0(^1A')$ transition. Nonaxial recoil and out-of-plane vibrations can decrease the anisotropy further.

Since the characteristic time to which the dissociation lifetime should be compared is the rotational period of the parent molecule, the effect of parent rotational temperature on the measured β is significant. For example, Hradil *et al.*[40] argue that the observed anisotropy parameter in NO_2 dissociation can vary from 1.4 to 0.6 in experiments carried out at 15 K and 370 K, respectively. Thus, if one were to derive the lifetimes of the excited state from the measured β ignoring the different rotational ''clocks,'' they would differ by almost an order of magnitude at these two temperatures.

Apart from the complexities in the interpretation of β outlined above, there are experimental difficulties in carrying out accurate measurements of product angular distributions. If the Doppler width of the optical transition in the interrogated product is comparable to or larger than the laser bandwidth (as in the case of hydrogen or CO correlated with ^{3}NH in our experiments) the full Doppler profile needs to be recorded by scanning the probe laser. When the spectrum of the product is not fully resolved (e.g., in the CO $B\leftarrow\leftarrow X$ transition), distortions due to partial capturing of the Doppler profiles of different product states may arise.

Although in our experiments the parent temperature is rather well defined and the β parameters are determined with good accuracy, one should not put excessive emphasis on the determination of the *absolute* dissociation lifetime in view of the above considerations. However, the *differences* in recoil anisotropies of products originating from different dissociation channels or at different excitation energies can serve as an excellent gauge of the *relative* time scales involved in the dissociation. For the perpendicular $S_1\leftarrow S_0$ transition in HNCO and under our expansion conditions ($T_{rot}=5$ K), $\beta>-0.23$ (the limiting value in the classical model discussed above) roughly corresponds to lifetimes longer than 5–10 ps, while $\beta\leqslant-0.6$ indicates dissociation in less than a picosecond. Below, we refer to images exhibiting β in the range 0 to -0.23 as isotropic.

B. Mechanistic interpretations

1. ^{1}NH+CO *channel*

The pathways leading to ^{1}NH+CO and their dependence on the one-photon photolysis energy are now rather well understood. While very near the threshold, decomposition proceeds via predissociation on S_0 following $S_1\rightarrow S_0$ IC,[17,24] at 230.1 nm [i.e., $\sim$700 cm^{-1} above $D_0(^1$NH+CO)] direct dissociation on S_1 prevails.[18,24] The barrier on S_1 to this channel was estimated at 400–600 cm^{-1},[24] in good agreement with recent calculations.[27,28]

The present experiments refine and add to this picture. Whereas previous work examined the low J states of CO, which are at the peak of the rotational distribution, Fig. 3 displays images recorded for $J>11$ states, which are in the low-population tail (the highest energetically accessible level is $J_{CO}=18$).[24] We show that although direct dissociation on S_1 dominates at this excitation energy, the S_0 pathway still makes a significant contribution, particularly to $J_{CO}>14$. In contrast to the images taken for low J_{CO}, which exhibit strong anisotropy characteristic of fast, direct dissociation on S_1 [e.g., Ref. 24 and Fig. 6(a)], $J_{CO}=14,15$ levels are formed more slowly, apparently via dissociation on S_0, resulting in an isotropic recoil distribution consistent with the isotropic images recorded for the hydrogen photofragments at comparable excitation energies (see below).

The reduced anisotropy may also result from the small fragment translational energy accompanying high CO rotational excitation. However, we favor the interpretation that two different PESs participate in the dissociation because of the fairly abrupt onset of the anisotropy in going from the image of $J_{CO}=14,15$ to that of $J_{CO}=12,13$. For $J_{CO}=12,13$ the direct S_1 pathway is dominant, as reflected in the large recoil anisotropy ($\beta<-0.6$) and ''cold'' rotational distribution of the correlated ^{1}NH products [Fig. 3(f)]. The small high-J tail in the CO rotational distribution from channel (3) is mainly due to dissociation on S_0. The ''warm'' rotational distribution of ^{1}NH correlated with $J_{CO}=14,15$, which extends to the energetic limit [Fig. 3(c)], supports this interpretation.

Finally, we note that the contribution of dissociation originating in $v_5=1$ of HNCO(S_0) to the observed J_{CO} signal is small and is significant only for $J_{CO}>12,13$ (Fig. 3). For $J_{CO}=16$ (not shown), this feature provides the main contribution to the population. The high value of β associated with it identifies its origin as direct dissociation on S_1.

The results shown in Figs. 4 and 5 better define the barrier height to ^{1}NH+CO dissociation on S_1. The nearly isotropic angular distribution in Fig. 4(c) suggests S_0 dissociation at $E_{avl}=411\,cm^{-1}$, while the high anisotropy of the angular distribution in Fig. 5(c), obtained for the adjacent peak in the ^{1}NH yield spectrum, indicates that direct S_1 dissociation prevails at $E_{avl}=524\,cm^{-1}$. In fact, the β parameter that fits the latter distribution is nearly identical to the one for $E_{avl}=705\,cm^{-1}$. We thus place the S_1 barrier to channel (3) dissociation at $470\pm60\,cm^{-1}$.

The excellent reproducibility of the β parameter values for the one-color experiments [$\beta=-0.84$, -0.81, and -0.78 for Figs. 4(d), 5(d), and 6(c), respectively] provides further confidence in our measurements. These values are closer to the limiting value of -1.0 than the previously reported value of -0.66 ± 0.05.[21] This is a result of the introduction of velocity map imaging and the better skimming of the molecular beam in our present setup, which lowered the rotational temperature of HNCO. The new value, $\beta=-0.80\pm0.05$, corresponds to a lifetime of 0.5 ± 0.3 ps for a 10 ± 5 K sample,[41] *provided β is determined exclusively by lifetime*.[33–37] The actual lifetime may be *shorter* if the measured β is reduced by other factors, and thus our limit of <1 ps is rather safe. We also note that at $\sim230\ cm^{-1}$ above the S_1 barrier, the yield of channel (3) is only few percent, and the most abundant product is NCO.[12] Therefore, the time scale of decay of S_1 reflects mainly the $S_1\rightarrow S_0$ IC rate.

2. H+NCO *channel*

Near its threshold, decomposition to the H+NCO channel proceeds via IC to S_0, and *ab initio* calculations predict a large barrier to this channel on S_1, i.e., $8\,700\ cm^{-1}$ (Ref. 28) or $11\,200\ cm^{-1}$ (Ref. 27).[17,18] While CO from channel (3) has a high recoil anisotropy at $\sim$230.1 nm, the hydrogen atom image at a comparable photolysis energy is isotropic [Fig. 2(b)]. This suggests that even after the opening of direct S_1 dissociation to channel (3), channel (2) decomposition still evolves more slowly on a different PES, presumably S_0, the results presented here show no recoil anisotropy in the hydrogen images up to $E_{avl}=8140\,cm^{-1}$, which sets a lower limit for the S_1 barrier to channel (2). As discussed above, IC from S_1 occurs in <1 ps; therefore, the isotropy of the H-atom images results from the S_0 lifetime. Such ''slow'' dissociation on S_0 (i.e., >5 ps lifetime) even at excess energies as high as $8000\ cm^{-1}$ is still compatible with model RRKM calculations carried out using reasonable transition state frequencies.[42] Note that since $S_1\rightarrow S_0$ IC requires an out-of-plane vibration of a'' symmetry, the β parameter may be further reduced.

Ab initio calculations reveal that the structure of the S_1 PES is rather complex,[27,28] having both *trans* and *cis* minima, with the former being the global minimum. The Franck-Condon region for one-photon $S_1\leftarrow S_0$ optical excitation is located near the *trans* well with strong gradients away from the *cis* configuration in the NCO bending coordinate. The two available high-level calculations give rather different energies for the *trans-cis* isomerization barrier ranging from $\sim8700\ cm^{-1}$ (Ref. 28) to $3500\ cm^{-1}$ (isomerization via HNC bend) or $7700\ cm^{-1}$ (isomerization via NCO bend) above the H+NCO asymptote.[27] The *trans* barriers to channel (2) dissociation are different in the two studies as well, as given at the beginning of the previous paragraph. However, both calculations show that the *cis* barrier to channel (2) dissociation is significantly lower than the *trans* one. It is placed at $4500\ cm^{-1}$ (Ref. 28) or at $6100\ cm^{-1}$ (Ref. 27). The one-photon dissociation results presented here are in agreement with the theoretical calculations for dissociation of the *trans* isomer.

While the mechanism of decomposition to channels (2) and (3) following one-photon excitation appears to be well understood, the corresponding VMP mechanism remains unsettled. Crim and co-workers observed a fourfold increase in the [channel (2)]:[channel (3)] ratio in photolysis experiments carried out following prior excitation of the $3\nu_1$ overtone of S_0, compared with the corresponding ratio obtained with one-photon excitation.[23] Both experiments were carried out at $\sim44\,400\ cm^{-1}$ excitation energy (225 nm).

Several scenarios for the VMP results are plausible. First, VMP may cause a change in the probability of $S_1\rightarrow S_0$ IC relative to direct dissociation on S_1. This can occur either via enhancement of the IC rate, or by reducing the direct S_1 coupling to the channel (3) continuum when a different region on S_1 is accessed by double-resonance optical excitation. In this scenario, the fraction of CO($X\,^1\Sigma^+$) arising from dissociation on S_0 would also increase compared to the value in the one-photon dissociation, and this may be evidenced by changes in β.

Another possible scenario involves the participation of the S_1 *cis* well in VMP. Note that $44\,400\ cm^{-1}$ excitation puts the molecule above the calculated S_1 barrier to channel (2) from the *cis* configuration.[27] Double-resonance excitation may thus open a direct dissociation route on S_1 to channel (2) from the *cis* isomer, thereby enhancing H+NCO formation. Isomerization from the *trans* to the *cis* isomer on S_1 following one-photon excitation is not likely, because the barrier may not have been exceeded and/or the bottleneck for isomerization should result in S_1 decay lifetimes longer than the observed <1 ps lifetime of the S_1 state. The experimental evidence to date is inconclusive, and further experiments (e.g., direct time-resolved measurements, or comparisons of recoil anisotropies obtained in one-photon dissociation and in VMP) should shed additional light on this issue.

3. ^{3}NH+CO *channel*

Channel (1) dissociation plays a role at all dissociation energies relevant to this study,[20–22] and must involve ISC to T_1—the only state correlating to ^{3}NH+CO products. Mebel *et al.* calculated an exit barrier of $1500\ cm^{-1}$ on the T_1 PES,[26] and the excitation energy used to obtain the image shown in Fig. 6 is $11\,800\ cm^{-1}$ above this barrier. Hence, dissociation on T_1 should be prompt. As seen in Fig. 6, with 230.1 nm photolysis channels (1) and (3) are associated with markedly different CO recoil anisotropies. Had ^{3}NH+CO evolved via direct $S_1\rightarrow T_1$ ISC, β would have been determined by the total removal rate of the S_1 state, yielding similar values for both channels. However, the isotropy of the channel (1) CO angular distributions indicates that an intermediate state whose lifetime exceeds 5 ps must exist on

the way from S_1 to T_1. The most plausible candidate is S_0, and hence the most likely dissociation route is $S_1 \rightarrow S_0 \rightarrow T_1 \rightarrow {}^3\mathrm{NH}+\mathrm{CO}$.

This conclusion is in accord with other observations: (i) The isotropic CO recoil is similar to that of the H atom produced in channel (2) via decomposition on S_0 at comparable photolysis energies. (ii) The state-specific effects previously observed in the yield spectra of the three channels near the ${}^1\mathrm{NH}+\mathrm{CO}$ threshold are rather similar for channels (1) and (2).[22] (iii) Pyrolysis of HNCO(S_0) yields ${}^3\mathrm{NH}+\mathrm{CO}$ as a major product,[25] in agreement with calculations,[43] demonstrating that $S_0 \rightarrow T_1$ coupling is possible. (iv) The observed increase in the NCO yield near its threshold with increasing photolysis energy can only be rationalized by assuming competition with another decay process on S_0, namely, ISC leading to channel (1).[29]

There are no symmetry restrictions on direct spin-orbit coupling between S_1 and T_1 (which have the same electronic configuration) in the C_s (or lower) symmetry point group of HNCO. However, the results of this work suggest that direct $S_1 \rightarrow T_1$ coupling is much weaker than $S_1 \rightarrow S_0$ IC. The reasons for this are not obvious *a priori*, because of the relative weakness of all the radiationless decay coupling strengths (especially at lower energies).[17] However, recent theoretical studies also indicate that direct $S_1 \rightarrow T_1$ coupling is inefficient at the energies employed here.[44]

V. SUMMARY AND CONCLUSIONS

The imaging results described in this paper provide a ''road map'' for the complex photoinitiated decomposition of HNCO into channels (1)-(3), which is applicable over a broad wavelength range. They pinpoint major mechanistic pathways and their dependence on energy, and photolysis energy regions in which competition among pathways is important. Since the mechanisms described here can be also used to rationalize previous data, it is useful to summarize briefly what is currently known and what remains to be unraveled.

Although the band origin of the $S_1 \leftarrow S_0$ transition is still unknown (a result of poor Franck-Condon factors), it is established that optical excitation in the wavelength region 280-193 nm accesses S_1.[11] All states reached via S_1 are dissociative, and at the longest excitation wavelengths (280-260 mm) ${}^3\mathrm{NH}$ is the only product. At low excitation energies, the ${}^3\mathrm{NH}$ yield spectra [channel (1)] are identical to the HNCO absorption spectrum (as monitored by two-photon LIF of HNCO).[17] The present results identify the channel (1) pathway as $S_1 \rightarrow S_0 \rightarrow T_1 \rightarrow {}^3\mathrm{NH}+\mathrm{CO}$. This mechanism can also explain the observed competition between channels (1) and (2) near the H+NCO threshold (at $\sim$260 nm).[29] The linewidths in the absorption and yield spectra reflect the $S_1 \rightarrow S_0$ IC process, whose time scale at the lowest end of the excitation wavelength range is >5 ps.[17,22] The spectra exhibit numerous state specific effects and perturbations.[17,22] Theoretical calculations reveal that only a small barrier to decomposition on T_1 exists, and that the T_1 origin lies several thousand wavenumbers below the S_1 origin.[26] Thus, dissociation to channel (1) will be controlled by the dynamics on the T_1 PES. It is noteworthy that even when the spin-allowed channels (2) and (3) are open, the spin-forbidden channel (1) is still observed, at least at wavelengths as short as 217 nm.[22]

The H+NCO channel first appears at its thermochemical threshold following dissociation on S_0 without a barrier.[17,18,29] The NCO rotational distributions near the channel (2) threshold can be fit well by phase space theory (PST) with strong angular momentum constraints.[29] The increase observed in the NCO yield with photolysis energy is rationalized by proposing that near the channel (2) threshold, the $S_0 \rightarrow T_1$ ISC rate is several fold faster than the channel (2) dissociation rate.[29]

The results reported here establish that at least up to 8140 cm^{-1} above the channel (2) threshold, this channel still evolves via radiationless decay, most likely on S_0, and this has to be taken into account in explaining the changes in branching ratios observed in VMP. Detailed studies of product energy disposal are needed for complete characterization of the transition state at higher energies. Likewise, accurate branching ratios between channels (1) and (2) as a function of energy are still unknown. The available results indicate that channel (1) is dominant in the region just above the opening of channel (2),[29] and is still significant (10%–20%) near the opening of channel (3), i.e., at $\sim$5000 cm^{-1} higher energy.[20,22] In order to better determine the separate rates of $S_0 \rightarrow T_1$ ISC and channel (2) dissociation, the total decay rate of S_0 and the branching ratios into channels (1) and (2) are required.

The ${}^1\mathrm{NH}+\mathrm{CO}$ channel is detected at its thermochemical threshold,[17,18] and it is concluded that the dissociation first takes place on S_0 without a significant barrier. Above a small barrier of $470 \pm 60\ \mathrm{cm}^{-1}$, direct dissociation on S_1 commences and quickly dominates.[17–19,24] Nevertheless, even 230 cm^{-1} above this barrier, the quantum yield of channel (3) is still small,[18] and the yield spectra monitored for all three channels are identical and exhibit many narrow features.[17,20,21] The dominant product is NCO, and the $S_1 \rightarrow S_0$ decay lifetime in this region is <1 ps. At higher photolysis energies, the coupling to the channel (3) continuum on S_1 increases rapidly, as evidenced by the sharp increase in the ${}^1\mathrm{NH}$ yield,[17,18] the decreasing yield of channel (2),[19] and the fast increase in linewidths in the ${}^1\mathrm{NH}$ yield spectrum.[17,20] More work is needed to characterize the relevant couplings and state-specific effects at wavelengths <230 nm.[22]

The channel (3) photodissociation dynamics on S_1 has been characterized (for one-photon excitation) at $E_{\mathrm{avl}}=700$ (230 nm) and 3200 cm^{-1} (217 nm). They are typical of direct, impulsive dissociation with most of the energy channeled into product translation.[16,21] These results, which are available both for global and correlated distributions, provide benchmarks for comparisons with dynamical calculations. Dissociation on S_1 to channel (2) at 193 nm, i.e., 13 000 cm^{-1} above $D_0(\mathrm{H}+\mathrm{NCO})$, gives rise to NCO with high bending excitation, but with most of the available energy in translation.[15]

The dynamics at excitation wavelengths <230 nm are presently the least well understood, although it is here that state- and bond-selective effects are identified both in one-photon dissociation and in VMP. In the VMP studies, changes in the NCO/^{1}NH and ^{3}NH/^{1}NH branching ratios are observed,[23,45] while in the one-photon dissociation experiments, the ^{3}NH yield spectrum progressively looses structure compared to the ^{1}NH yield spectrum.[22] It is also in this region that the *cis-trans* isomerization barrier on S_1 is exceeded,[27,28] and the coupling to T_1 via ISC to T_2 may becomes important, as suggested recently.[44]

In a previous publication we hypothesized that in this region, ISC along the N-C coordinate on S_1 occurs predominantly in the Franck-Cordon region, i.e., at N-C separations which are *compressed* compared to the S_1 equilibrium internuclear separation.[22] We also suggested that when S_1 dissociation to channel (3) is fast, the decomposing system does not return to the PES region where ISC is efficient, resulting in a time scale for ISC that is shorter than the time scales for IC and/or dissociation on S_1 to channel (3). Such a mechanism can rationalize the selective loss of structure in the ^{3}NH yield spectra. In view of the the results presented here, which are in agreement with recent calculations by Morokuma and co-workers,[44] we modify the proposed mechanism to include competition between the $S_1 \rightarrow T_2 \rightarrow T_1$ and the $S_1 \rightarrow S_0 \rightarrow T_1$ pathways at short wavelengths, with the former increasing in importance at wavelengths <230 nm. Morokuma and co-workers find that the $S_1 \rightarrow T_2 \rightarrow T_1$ crossing occurs at N-C separations shorter than the S_1 equilibrium, and the $S_1 \rightarrow S_0 \rightarrow T_1$ crossing regions are all at N-C internuclear distances greater than equilibrium, in agreement with our proposed model. The existence of two pathways terminating in T_1 may lead to interference, which can additionally contribute to the loss of structure in the ^{3}NH yield spectra. Clearly, further investigation of this photolysis energy region is needed. The role of the *cis*-isomer in VMP also awaits clarification as discussed in Sec. IV.

ACKNOWLEDGMENTS

We wish to thank F. F. Crim, R. Schinke, K. Morokuma, A. Sanov, I. Bezel, R. Cao, and C. Wittig for helpful discussions, and K. Morokuma for communicating results prior to publication. Support by the National Science Foundation is gratefully acknowledged.

[1] R. Schinke, *Photodissociation Dynamics* (University Press, Cambridge, 1993).
[2] E. S. Medvedev and V. I. Osherov, *Radiationless Transitions of Polyatomic Molecules* (Springer, Berlin, 1995).
[3] S. Williams, J. D. Tobiason, J. R. Dunlop, and E. A. Rohlfing, J. Chem. Phys. **102**, 8342 (1995); J. D. Tobiason, J. R. Dunlop, and E. A. Rohlfing, *ibid.* **103**, 1448 (1995); D. W. Neyer, X. Luo, P. L. Houston, and I. Burak, *ibid.* **98**, 5095 (1993); **102**, 1645 (1995).
[4] A. Geers, J. Kappert, F. Temps, and J. W. Weibrecht, J. Chem. Phys. **93**, 1472 (1990); **98**, 4297 (1993); **99**, 2271 (1993); **101**, 3618 (1994); **101**, 3634 (1994).
[5] B. R. Foy, M. P. Casassa, J. C. Stephenson, and D. S. King, J. Chem. Phys. **90**, 7037 (1989); **92**, 2782 (1990).
[6] M. H. Alexander, H.-H. Werner, and P. J. Dagdigian, J. Chem. Phys. **89**, 1388 (1989); M. H. Alexander, H.-H. Werner, T. Hemmer, and P. J. Knowles, *ibid.* **93**, 3307 (1990).
[7] M. Stumpf, A. J. Dobbyn, D. H. Mordaunt, H.-M. Keller, H. Fluethmann, R. Schinke, H.-J. Werner, and K. Yamashita, Faraday Discuss. Chem. Soc. **102**, 193 (1995).
[8] (a) W. H. Green, Jr., C. B. Moore, and W. F. Polik, Annu. Rev. Phys. Chem. **43**, 591 (1992), and references therein; (b) S. A. Reid and H. Reisler, *ibid.* **47**, (1996), and references therein; **47**, 495 (1996), and references therein.
[9] K. Mikhaylichenko, C. Riehn, L. Valachovic, A. Sanov, and C. Wittig, J. Chem. Phys. **105**, 6807 (1996).
[10] (a) R. N. Zare and D. R. Herschbach, Proc. IEEE **51**, 173 (1963); (b) R. N. Zare, Mol. Photochem. **4**, 1 (1972).
[11] R. N. Dixon and G. H. Kirby, Trans. Faraday Soc. **64**, 2002 (1968).
[12] (a) T. A. Spiglanin, R. A. Perry, and D. W. Chandler, J. Phys. Chem. **90**, 6184 (1986); (b) T. A. Spiglanin and D. W. Chandler, Chem. Phys. Lett. **141**, 428 (1987); (c) T. A. Spiglanin, R. A. Perry, and D. W. Chandler, J. Chem. Phys. **87**, 1568 (1987); (d) T. A. Spiglanin and D. W. Chandler, *ibid.* **87**, 1577 (1987).
[13] W. K. Yi and R. Bersohn, Chem. Phys. Lett. **206**, 365 (1993).
[14] B. Ruscic and J. Berkowitz, J. Chem. Phys. **100**, 4498 (1994).
[15] J. Zhang, M. Dulligan, and C. Wittig, J. Phys. Chem. **99**, 7446 (1995).
[16] M. Kawasaki, Y. Sato, K. Suto, Y. Matsumi, and S. H. S. Wilson, Chem. Phys. Lett. **251**, 67 (1996).
[17] (a) M. Zyrianov, A. Sanov, Th. Droz-Georget, and H. Reisler, Soc. Chem. Faraday Discuss. **102**, 263 (1995); (b) M. Zyrianov, Th. Droz-Georget, A. Sanov, and H. Reisler, J. Chem. Phys. **105**, 8111 (1996).
[18] S. S. Brown, H. L. Berghout, and F. F. Crim, J. Chem. Phys. **105**, 8103 (1996); S. S. Brown, R. B. Metz, H. L. Berghout, and F. F. Crim, J. Phys. Chem. **100**, 7948 (1996); S. S. Brown, H. L. Berghout, and F. F. Crim, J. Chem. Phys. **102**, 8440 (1995).
[19] (a) R. A. Brownsword, T. Laurent, R. K. Vatsa, H.-R. Volpp, and J. Wolfrum, Chem. Phys. Lett. **249**, 162 (1996); (b) **258**, 164 (1996); (c) R. A. Brownsword, M. Hillenkamp, T. Laurent, R. K. Vatsa, and H.-R. Volpp, J. Chem. Phys. **106**, 4436 (1997).
[20] Th. Droz-Georget, M. Zyrianov, A. Sanov, and H. Reisler, Ber. Bunsenges. Phys. Chem. **101**, 469 (1997).
[21] A. Sanov, Th. Droz-Georget, M. Zyrianov, and H. Reisler, J. Chem. Phys. **106**, 7013 (1997).
[22] M. Zyrianov, Th. Droz-Georget, and H. Reisler, J. Chem. Phys. **106**, 7454 (1997).
[23] S. S. Brown, R. B. Metz, H. L. Berghout, and F. F. Crim, J. Phys. Chem. **105**, 6293 (1996).
[24] Th. Droz-Georget, M. Zyrianov, H. Reisler, and D. W. Chandler, Chem. Phys. Lett. **276**, 316 (1997).
[25] (a) O. Kajimoto, O. Koudo, K. Okada, J. Fujikane, and T. Fueno, Bull. Chem. Soc. J. **58**, 3469 (1985); (b) J. D. Mertens, A. Y. Chang, R. K. Hanson, and C. T. Bowman, Int. J. Chem. Kinet. **29**, 1049 (1989).
[26] A. M. Mebel, A. Luna, M. C. Lin, and K. Morokuma, J. Chem. Phys. **105**, 6439 (1996).
[27] J. E. Stevens, Q. Cui, and K. Morokuma, J. Chem. Phys. **108**, 1452 (1998).
[28] J. Klossika, H. Floethmann, C. Beck, R. Schinke, and K. Yamashita, Chem. Phys. Lett. **276**, 325 (1997).
[29] M. Zyrianov, Th. Droz-Georget, A. Sanov, and H. Reisler (to be published).
[30] H. H. Parker and A. Eppink, J. Chem. Phys. **107**, 2357 (1997); Rev. Sci. Instrum. **68**, 3477 (1997).
[31] R. N. Bracewell, *The Fourier Transform and its Applications* (McGraw-Hill, New York, 1986).
[32] R. G. Bray and R. M. Hochstrasser, Mol. Phys. **31**, 1199 (1976).
[33] R. J. Gordon and G. E. Hall, Adv. Chem. Phys. **XCVI**, 1 (1996).
[34] R. Liyanage and R. J. Gordon, J. Chem. Phys. **107**, 7209 (1997).
[35] C. Jonah, J. Chem. Phys. **55**, 1915 (1971).
[36] G. E. Busch and K. R. Wilson, J. Chem. Phys. **56**, 3638 (1972).
[37] S. Yang and R. Bersohn, J. Chem. Phys. **61**, 4400 (1974).
[38] S. Mukamel and J. Jortner, J. Chem. Phys. **61**, 5348 (1974).
[39] T. J. Butenhoff, K. L. Careton, R. D. van Zee, and C. B. Moore, J. Chem. Phys. **94**, 1947 (1991).
[40] V. P. Hradil, T. Suzuki, S. A. Newitt, B. J. Whitaker, and P. L. Houston, J. Chem. Phys. **99**, 4455 (1993).
[41] A. Sanov, Ph.D. thesis, University of Southern California, 1996.
[42] In these estimates the parent density of states was calculated by direct harmonic count. The H-NCO transition state frequencies were taken as those of free NCO (2340 cm^{-1}, 1290 cm^{-1}, and 680 cm^{-1}), and 100–200 cm^{-1} for both the in-plane and out-of-plane H-N-C bending vibrations. At $E_{avl}=8000\ cm^{-1}$ these parameters give rates that are smaller than

$\sim 10^{11}\,s^{-1}$ and can lead to isotropic recoil distributions. Note that the parent density of states may be greatly underestimated due to the neglect of anharmonicities and the existence of several HNCO isomers, which would contribute to the S_0 density of states at high energies.

[43] W.-H. Fang, X.-Z. You, and Z. Yin, Chem. Phys. Lett. **238**, 236 (1995).
[44] K. Morokuma (private communication, 1998).
[45] H. L. Berghout, S. S. Brown, R. Delgado, and F. F. Crim, J. Chem. Phys. **109**, 2257 (1998).